Title: Circuit and synaptic organization of forebrain-to-midbrain pathways that promote and suppress vocalization

Running title: Inhibitory neurons push and pull the midbrain USV circuit

Valerie Michael[1*], Katherine Tschida[1*], Jack Goffinet[1], John Pearson[1], Fan Wang[1], Richard Mooney[1]

[1]Department of Neurobiology, Duke University Medical Center, Durham, NC 27710

[*]Co-first Authors

Lead contact: Richard Mooney, email: mooney@neuro.duke.edu

Abstract

Animals vocalize only in certain behavioral contexts, but the circuits and synapses through which forebrain neurons trigger or suppress vocalization remain unknown. Here we used transsynaptic tracing to identify two populations of inhibitory neurons that lie upstream of neurons in the periaqueductal gray that gate the production of ultrasonic vocalizations in mice (i.e., PAG-USV neurons). Activating PAG-projecting neurons in the preoptic hypothalamus (POA_{PAG} neurons) elicited USV production in the absence of social cues. In contrast, activating PAG-projecting neurons in the extended amygdala (EA_{PAG} neurons) transiently suppressed USV production without disrupting non-vocal social behavior. Optogenetics-assisted circuit mapping in brain slices revealed that POA_{PAG} neurons directly inhibit PAG interneurons, which in turn inhibit PAG-USV neurons, whereas EA_{PAG} neurons directly inhibit PAG-USV neurons. These experiments identify two major forebrain inputs to the PAG that trigger and suppress vocalization, respectively, while also establishing the synaptic mechanisms through which these neurons exert opposing behavioral effects.

Keywords: vocalization, ultrasonic, preoptic, hypothalamus, amygdala, periaqueductal gray

Introduction

The decision to vocalize is often a matter of life and death, as vocalizations are an important medium for sexual and social signaling between conspecifics but may also inadvertently advertise the caller's location to eavesdropping predators. Consequently, many factors influence the decision to vocalize, including the presence of external sensory and social cues, as well as the animal's own internal state and past experience. Work from the last five decades has established the midbrain periaqueductal gray (PAG) as an obligatory gate for the production of vocalizations in all mammals (Jurgens, 1994, 2002, 2009), and it is thought that forebrain inputs to the PAG regulate the production of vocalizations in a context-dependent fashion. In line with this idea, forebrain regions including the anterior cingulate cortex, amygdala, and hypothalamus have been implicated in regulating vocalization as a function of social context (Bennett et al., 2019; Dujardin and Jurgens, 2006; Gao et al., 2019; Green et al., 2018; Jurgens, 1982, 2002; Kyuhou and Gemba, 1998; Ma and Kanwal, 2014; Manteuffel et al., 2007). Notably, although electrical or pharmacological activation of a variety of forebrain regions can elicit vocalization (Jurgens, 2009; Jurgens and Ploog, 1970; Jurgens and Richter, 1986), these effects depends on an intact PAG (Jurgens and Pratt, 1979; Lu and Jurgens, 1993; Siebert and Jurgens, 2003), suggesting that the PAG acts as an essential hub for descending forebrain control of vocalization. However, the circuits and synapses through which forebrain neurons interact with the PAG vocal gating circuit to either promote or suppress vocalization remain entirely unknown.

A major challenge to understanding the circuit and synaptic mechanisms through which descending forebrain neurons influence vocalization was that, until recently, the identity of the PAG neurons that play an obligatory role in vocal gating remained unknown. The PAG is a functionally heterogeneous structure important to many survival behaviors (Bandler and Shipley, 1994; Carrive, 1993; Evans et al., 2018; Holstege, 2014; Tovote et al., 2016), thus hindering the identification of vocalization-related PAG neurons and forebrain inputs to these neurons that

might influence vocalization. To overcome this challenge, we recently used an intersectional technique to identify neurons in the PAG of the mouse that gate the production of ultrasonic vocalizations (USVs) (i.e., PAG-USV neurons (Tschida et al., 2019)), which mice produce in a variety of social contexts (Chabout et al., 2015; Holy and Guo, 2005; Maggio and Whitney, 1985; Neunuebel et al., 2015; Nyby et al., 1979; Portfors and Perkel, 2014; Whitney et al., 1974). The identification of PAG-USV neurons opens the door to identifying their proximal upstream inputs and to understanding how these inputs influence both vocal behavior as well as neural activity within the PAG vocal gating circuit.

In the current study, we used transsynaptic tracing to identify neurons that provide direct input to PAG-USV neurons, as well as to GABAergic interneurons in the PAG which we show inhibit PAG-USV neurons. Using this transsynaptic approach as an entry point, we identified inhibitory neurons in both the hypothalamus and the amygdala that provide synaptic input to the PAG vocal gating circuit. We then tested the role of these upstream neurons in shaping vocal behavior and characterized the synaptic mechanisms through which these two populations of inhibitory neurons act on the midbrain vocal gate to exert opposing effects on USV production.

Results

Inhibitory neurons in the hypothalamus and amygdala provide input to the PAG vocal gating circuit

To identify forebrain neurons that provide input to the PAG vocal gating circuit, we performed transsynaptic tracing from PAG-USV neurons, which are primarily glutamatergic (Tschida et al., 2019). Briefly, to label inputs to PAG-USV neurons, we used an activity-dependent labeling strategy (CANE; see Methods) to express Cre-dependent helper viruses in PAG-USV neurons (Rodriguez et al., 2017; Sakurai et al., 2016; Tschida et al., 2019). A pseudotyped replication-

deficient rabies virus was subsequently injected into the PAG, allowing selective transsynaptic labeling of direct inputs to PAG-USV neurons (Fig. 1A, see Methods). Because the activity of many glutamatergic PAG neurons is shaped by potent inhibition from GABAergic PAG neurons (Tovote et al., 2016), we also performed transsynaptic tracing from nearby GABAergic PAG neurons that likely provide inhibition onto PAG-USV neurons (and see below for related data). To label direct inputs to nearby GABAergic PAG neurons, Cre-dependent helper viruses were injected into the caudolateral PAG of a VGAT-Cre mouse, and a pseudotyped replication-deficient rabies virus was subsequently injected at the same site to enable transsynaptic tracing from these cells (Fig. 1B). These rabies tracing experiments revealed monosynaptic inputs to PAG-USV neurons as well as to nearby GABAergic PAG neurons from a variety of forebrain areas (Table 1), including the hypothalamus and amygdala. We subsequently focused on neurons in these latter two regions, as our preliminary studies revealed that they can exert robust effects on vocal behavior (see below).

Within the hypothalamus, we observed dense labeling of neurons in the medial preoptic area (POA, Fig. 1A-B), a region that plays a crucial role in sexual behavior (Balthazart and Ball, 2007; McKinsey et al., 2018; Newman, 1999; Wei et al., 2018) and more specifically in the production of courtship vocalizations in rodents and in songbirds (Alger and Riters, 2006; Bean et al., 1981; Floody, 1989, 2009; Floody et al., 1998; Fu and Brudzynski, 1994; Gao et al., 2019; Riters and Ball, 1999; Vandries et al., 2019). Within the amygdala, we observed dense inputs to both PAG cell types from neurons spanning the most medial and rostral portions of the amygdala (referred to here as the extended amygdala (EA), see below) continuing caudally to the central amygdala (CeA) (Fig. 1A-B). Given the role of the amygdala in anxiety and fear-related behaviors (Duvarci and Pare, 2014; Ehrlich et al., 2009; Janak and Tye, 2015; LeDoux, 2007), we hypothesized that these amygdalar inputs to the PAG vocal gating circuit would

suppress the production of USVs, and that preoptic and amygdala inputs to the PAG vocal gating circuit would exert contrasting effects on vocal behavior.

To characterize the neurotransmitter phenotypes of these upstream hypothalamic and amygdalar neurons, we performed two-color *in situ* hybridization on transsynaptically labeled neurons for mRNA transcripts expressed in glutamatergic and GABAergic cells (vesicular glutamate transporter (vGluT2) and vesicular GABA transporter (VGAT); Fig. 1C, see Methods). This experiment revealed that the majority (~84%, Fig. 1C-D) of PAG-projecting POA neurons (i.e. POA_{PAG} neurons) and almost all (~98%, Figure 1D) of PAG-projecting EA and CeA neurons (i.e. EA_{PAG} and CeA_{PAG} neurons) are GABAergic. In summary, the PAG vocal gating circuit receives input from inhibitory neurons in both the preoptic hypothalamus and the amygdala.

Activating PAG-projecting POA neurons elicits USVs in the absence of social cues

The POA plays a crucial role in courtship, raising the possibility that POA_{PAG} neurons are important to promoting USV production. To test this idea, we selectively expressed channelrhodopsin (ChR2) in POA_{PAG} neurons, by injecting a Cre-dependent AAV driving ChR2 expression into the POA and injecting a retrogradely-infecting AAV that drives Cre expression into the caudolateral PAG, the region in which PAG-USV neurons are concentrated (Fig. 2A). Optogenetic activation of POA_{PAG} cell bodies was sufficient to elicit USVs in isolated male mice (USVs elicited in N=6 of 8 males; 10 Hz trains or tonic pulses of 1-2s duration; Fig. 2A, Movie S1). We also observed that activation of POA_{PAG} neurons was sufficient to elicit USVs from female mice (N=3 of 4 mice), indicating that POA_{PAG} neurons are capable of promoting USV production in both males and females.

To begin to describe the molecular phenotype of POA_{PAG} neurons, we performed in situ hybridization on POA_{PAG} neurons, which established that the majority of these cells express VGAT (Fig. 2B), similar to the POA neurons that are labeled via transsynaptic tracing from the

PAG vocal gating circuit. We also noted that the majority of POA_{PAG} neurons express Estrogen Receptor 1 (Esr1), a prominent marker for neurons in the POA (~86%, Fig. 2B) (Fang et al., 2018; Moffitt et al., 2018; Wei et al., 2018). Given this finding, we next tested whether optogenetic activation of Esr1+ POA neurons was sufficient to elicit USV production, by injecting a Cre-dependent AAV driving the expression of ChR2 into the POA of Esr1-Cre mice. We observed that optogenetically activating $Esr1^+$ POA neurons was sufficient to elicit USV production in both singly tested male (N=4 of 5) and female mice (N=3 of 4) (Fig. 2C). Finally, to test whether activation of the $Esr1^+$ POA neurons that project to the PAG is sufficient to elicit USVs, we optogenetically activated the axon terminals of $Esr1^+$ POA neurons within the PAG (Fig. 2D). Bilateral $Esr1^+$ POA_{PAG} terminal activation within the PAG was sufficient to elicit USV production (N=1 of 2 males; N=4 of 6 females, 20 Hz trains of 2-10s duration), though we also noted optogenetically-elicited escape behaviors in 4 of 8 of the tested animals, which suggests that there is functional heterogeneity in $Esr1^+$ PAG-projecting neurons of the POA and nearby regions. Taken together, these experiments show that activation of GABAergic, $Esr1^+$ POA_{PAG} neurons is sufficient to elicit USV production.

The findings that POA neurons directly innervate the PAG vocal gating circuit and that activating $Esr1^+$ POA_{PAG} neurons readily triggers USV production support the idea that $Esr1^+$ POA neurons act directly on the vocal gating mechanism in the PAG, rather than through an indirect process, perhaps involving hedonic reinforcement. To control for this possibility, we performed real-time place preference tests in which optogenetic stimulation of either POA_{PAG} or $Esr1^+$ POA neurons was applied when mice were in only one of two sides of the test chamber. We observed that optogenetic activation of $Esr1^+$ POA neurons did not positively reinforce place preference (mean PP=0.46 +/- 0.02 for N=5 mice) and that in fact, activating POA_{PAG} neurons drove a slightly negative place preference on average (mean PP=0.39 +/- 0.07 for N=7 mice; Fig. S1A). We also note that when using the same stimulation parameters that were sufficient to

elicit USVs, optogenetic activation of either POA_{PAG} or $Esr1^{+}$ POA neurons did not drive mounting of other mice (data not shown; N=7 POA_{PAG}-ChR2 mice tested; N=4 POA-Esr1-ChR2 mice tested) nor did it induce overt locomotion (Fig. S1B). These experiments indicate that activation of POA_{PAG} neurons can elicit USVs independently of other courtship behaviors and without putting mice in a positive hedonic state.

Because the POA lies upstream of the PAG, we anticipated that optogenetic activation of the POA would elicit USV production at longer latencies than observed for optogenetic activation of PAG-USV neurons. Indeed, we found that the minimum and mean latencies to elicit USVs by optogenetic stimulation of POA neurons were 664.5 +/- 320.9 ms and 1782.6 +/- 407.6 ms respectively (Fig. S2, calculated from N=9 POA_{PAG}-ChR2 and N=7 POA-Esr1-ChR2 mice), and we note that these latencies are longer than those observed when optogenetically activating PAG-USV neurons (PAG-USV activation: min. latency from laser onset to first USV was 23.4 ± 8.6 ms, mean latency was 406.6 ± 0.5 ms) (Tschida et al., 2019). We also found that USV bouts elicited by optogenetic activation of the POA often outlasted the duration of the optogenetic stimulation, sometimes by many seconds (Figs. 2, S2). This contrasts with what is observed following optogenetic activation of PAG-USV neurons, in which USV bout durations map on tightly to the duration of optogenetic stimulation (Tschida et al., 2019), and suggests that brief optogenetic stimulation in the POA can be transformed into longer-lasting changes in neural activity within the POA network or across POA-to-PAG synapses.

Acoustic characterization of USVs elicited by activation of POA neurons

Given the artificial nature of optogenetic stimulation, we wondered whether USVs elicited by optogenetic activation of POA neurons were acoustically similar to the USVs that are normally produced by mice during social interactions. To compare the acoustic features of optogenetically-elicited USVs (opto-USVs) to those of USVs produced spontaneously to a nearby female, we employed a recently described method using variational autoencoders

(VAEs) (Goffinet, 2019; Sainburg et al., 2019). Briefly, the VAE is an unsupervised modeling approach that uses spectrograms of vocalizations as inputs and from these data learns a pair of probabilistic maps, an “encoder” and a “decoder,” capable of compressing vocalizations into a small number of latent features while attempting to preserve as much information as possible (Fig. 3A-B). Notably, this method does not rely on user-defined acoustic features, nor does it require clustering of vocalizations into categories. We applied this approach to spectrograms of USVs to compare the acoustic features of female-directed and opto-USVs from the same mice and found that the VAE converged on a concise representation of only five dimensions (data not shown). We then employed a dimensionality reduction method known as UMAP (McInnes, 2018) to visualize the latent features of these USVs in 2D space (Fig. 3C). This analysis revealed that for some mice, female-directed and opto-USVs were acoustically similar (Fig. 3C, left), while for other mice, a subset of opto-USVs were acoustically distinct from female-directed USVs (Fig. 3C, right). To quantify the difference between female-directed and opto-USVs for each mouse, we estimated the Maximum Mean Discrepancy (Gretton, 2012) between distributions of latent syllable representations as in (Goffinet, 2019). In addition, a baseline level of variability in syllable repertoire was established for each mouse by estimating the MMD between the first and second halves of female-directed USVs emitted in a recording session (Fig. 3D). A paired comparison revealed significantly larger differences between female-directed and opto-USVs than expected by variability within the female-directed recording sessions alone (Fig. 3D, two-sided, continuity-corrected Wilcoxon signed-rank test, $W=5$, $p<1e-2$), or than expected by across-day variability in female-directed recording sessions from control animals (gray points, Fig. 3D, female-directed USVs were recorded on 2 different days from $N=10$ control mice, $p=0.003$ for difference between female-directed vs. female-directed in control mice and opto vs. female-directed in experimental mice, Mann Whitney U test). In conclusion, many USVs elicited by optogenetic activation of POA neurons resemble female-directed USVs,

although a subset differs in their acoustic features from USVs found in the animals' female-directed repertoires.

We next sought to understand in more detail exactly how these acoustically unusual opto-USVs differed from natural USVs. When the latent representations of these two types of USVs were plotted together for all mice in our dataset, it became clear that opto-USVs and female-directed USVs are largely acoustically overlapping except in one region of the UMAP representation (upper middle portion of Fig. 3E, dominated by blue points). Despite this outlying region of acoustically distinct opto-USVs, we conservatively estimate that only 20% of condition information (optogenetically-elicited versus female-directed) can be predicted by latent syllable descriptions, consistent with largely overlapping distributions of natural and opto-USVs (0.20 bits, 5-fold class-balanced logistic regression). We then re-plotted UMAP representations of only the opto-USVs, with each USV syllable color-coded according to syllable energy (i.e., amplitude, Fig. 3F, left) or frequency bandwidth (Fig. 3F, right). This analysis revealed that the acoustically unusual opto-USVs tended to be very loud and also had high frequency bandwidth. Visual inspection of spectrograms of opto-USVs also confirmed that those that did not overlap acoustically with natural USVs tended to be louder and have higher frequency bandwidths (Fig. 3F, bottom, opto 1 and opto 2), while opto-USVs that overlapped with natural USVs did not possess these unusual acoustic features (Fig. 3F, bottom, opto 3). To determine whether the differences between optogenetically-elicited and natural USVs were consistent across mice, we summarized each recording session by the mean latent representation of its syllables, and then summarized the shift from natural to optogenetically-elicited syllable repertoires by the corresponding vector between summary points. A shuffle test revealed significantly larger alignment between these vectors than expected by chance (mean cosine similarity=0.50, $p<1e-5$), indicating that opto-USVs differed from female-directed USVs in a manner that was consistent across mice. In summary, optogenetic activation of the POA elicits USVs whose

acoustic features are largely overlapping with those of female-directed USVs produced by the same animal, despite the artificiality inherent to optogenetic stimulation.

Activating PAG-projecting EA neurons transiently suppresses USV production

We next sought to understand how PAG-projecting amygdala neurons contribute to vocalization. We began with a viral strategy designed to express ChR2 in PAG-projecting EA and CeA neurons, by injecting a Cre-dependent AAV driving ChR2 expression targeted to the amygdala and then injecting AAV-retro-Cre into the PAG (Fig. 4). Surprisingly, given the strong transsynaptic labeling of both the CeA and EA achieved with modified rabies tracing from the PAG vocal gating circuit, we found that this viral strategy failed to label neurons in the CeA and instead only labeled EA neurons, whose cell bodies reside medial to the CeA and dorsal to the medial amygdala (Figs. 4A, S3). To ensure that this labeling pattern was due to restricted tropism of the AAV-retro-Cre virus and not to inaccurate targeting of the CeA, we repeated the injections of the AAV-retro-Cre virus in the PAG of a Cre-dependent tdTomato reporter mouse. Again, we observed cell body labeling in the EA but not in the CeA (Fig. S4), suggesting that in contrast to modified rabies virus used in the transsynaptic tracing from the PAG vocal gating circuit, the AAV-retro-Cre virus can infect EA but not CeA neurons.

To test whether PAG-projecting EA neurons contribute to vocalization, we first tested the effects of optogenetically activating these neurons in isolated mice. Optogenetic activation of EA_{PAG} neurons failed to elicit USV production and also did not drive any other overt behavioral effects (data not shown). However, when EA_{PAG} neurons were optogenetically activated in male mice that were actively courting females and vocalizing, USV production was immediately and reversibly suppressed (Fig. 4B, N=8 mice). This suppressive effect was restricted to the period when EA_{PAG} neurons were being optogenetically stimulated, and USV production rebounded following the end of the optogenetic stimulation period (Fig. 4B). After using in situ hybridization to confirm that most EA_{PAG} neurons are inhibitory (~92% express VGAT, Fig. 4C), we next

employed a related viral strategy to express ChR2 selectively in GABAergic EA_{PAG} neurons (Fig.4D, AAV-retro-FLEX-ChR2 injected into the PAG of a VGAT-Cre mouse). With this strategy, we found that optogenetic activation of GABAergic EA_{PAG} neurons robustly suppressed USV production (Fig. 4D, N=4 mice). Finally, we tested the effects on vocal behavior of optogenetically activating the axon terminals of GABAergic EA_{PAG} neurons within the PAG (Fig. 4D). Such bilateral terminal activation was also sufficient to suppress USV production (in N=3 of 3 males; Fig. 4D).

One possibility is that activating EA_{PAG} neurons suppresses USV production by putting the mouse into a fearful or aversive state, rather than through a direct suppressive effect of EA_{PAG} neurons on the PAG vocal gating circuit. To test this idea, we carefully examined the non-vocal behaviors of male mice during optogenetic activation of EA_{PAG} neurons. Mice exhibited neither freezing nor fleeing during optogenetic stimulation, and more notably, they usually continued to follow and sniff the female during the laser stimulation periods (Movie S2; distance between male and female did not increase during optogenetic stimulation, Fig. S1B). We also confirmed that the change in USV production rates driven by the optogenetic activation of EA_{PAG} neurons was different from the change in USV rates over time in mice that didn't receive laser stimulation (Fig. 4D, black trace), the change in USV rates over time in GFP control mice (Fig. 4D, green trace), and the change in USV rates over time in EA_{PAG} -ChR2-expressing mice that were connected to a dummy ferrule that only shined blue light over their head (Fig. 4D, gray trace; $p<0.01$ for differences between ChR2 groups vs. control groups during laser time, one-way ANOVA followed by post-hoc pairwise Tukey's HSD tests). Finally, we performed real-time place preference tests in which EA_{PAG} neurons were optogenetically activated when mice were in one of two sides of a test chamber (EA_{PAG} neurons were labeled with either the AAV-retro-Cre or the AAV-retro-ChR2 viral strategies). This experiment revealed that activation of EA_{PAG} neurons does not drive a negative place preference (Fig. S1A). In summary, our data support

the idea that activating EA_{PAG} neurons transiently and selectively suppresses USVs produced by male mice during courtship, and that this effect cannot be accounted for by the mouse being put into a fearful or aversive state.

Axonal projections of POA_{PAG} and EA_{PAG} neurons

To further characterize the anatomy of POA_{PAG} and EA_{PAG} neurons, we used intersectional methods to label these neurons with GFP and tdTomato respectively and traced their axonal projections throughout the brain (Fig. S5, AAV-retro-Cre injected into caudolateral PAG, AAV-FLEX-GFP into POA, AAV-FLEX-tdTomato into EA). We observed dense projections from both POA_{PAG} and EA_{PAG} neurons to a variety of dopaminergic cell groups, including the VTA, SNc and retrorubral/A8 region. We also note that EA_{PAG} neurons provide input to the lateral preoptic area (Fig. S5, top left), while POA_{PAG} neurons provide input to the same region in which EA_{PAG} cell bodies reside (Fig. S5, middle left). We also observed projections of both cell groups to the parabrachial nucleus and Barrington's nucleus (data not shown), as well as dense and overlapping terminal fields within the caudolateral PAG (Fig. S5, bottom right).

Synaptic interactions between POA_{PAG} and EA_{PAG} neurons and the PAG vocal gating circuit

The functional and anatomical experiments described above establish that two different populations of inhibitory forebrain neurons provide input to the PAG vocal gating circuit, one of which (the POA) promotes USV production in the absence of any social cues, while the other (the EA) suppresses spontaneous USVs produced by male mice during courtship. To understand how two different inhibitory inputs to the PAG can exert opposing effects on vocal behavior, we performed ChR2-assisted circuit mapping experiments in brain slices to characterize the properties of POA and EA synapses onto PAG-USV neurons and nearby GABAergic PAG neurons. Given that optogenetic activation of GABAergic EA_{PAG} neurons

suppresses USV production, we predicted that GABAergic EA neurons directly inhibit PAG-USV neurons. To test this idea, we performed whole-cell patch clamp recordings from PAG-USV neurons while optogenetically activating EA_{PAG} axons within the PAG. Briefly, AAV-FLEX-ChR2 was injected into the EA of a VGAT-Cre;Fos-dsTVA crossed mouse in order to express ChR2 in GABAergic EA_{PAG} axon terminals within the PAG. After four weeks, we used the CANE method to infect PAG-USV neurons with a pseudotyped CANE-rabies virus driving the expression of mCherry (CANE-RV-mCherry, Fig. 5A-B, see Methods). We visually targeted our recordings to mCherry-expressing PAG-USV neurons and optogenetically activated EA terminals in the presence of TTX and 4AP in order to isolate monosynaptic pathways (Fig. 5C-D). Activating EA_{PAG} terminals evoked IPSCs in 16 of 29 of the mCherry-labeled PAG-USV neurons from which we recorded (mean current=180.3 pA at 0 mV in TTX/4AP). These evoked currents were completely abolished by application of gabazine, a $GABA_A$ receptor antagonist (Fig. 5E-F). These findings indicate that EA_{PAG} activity suppresses ongoing vocalizations by directly inhibiting PAG-USV neurons.

Given that activating GABAergic POA_{PAG} neurons elicits vocalization (Fig. 2), and that the majority of PAG-USV neurons are glutamatergic (Tschida et al., 2019), we hypothesized that POA_{PAG} axons act via local interneurons in the PAG to disinhibit PAG-USV neurons. To test this hypothesis, we first performed whole-cell patch clamp recordings from GABAergic PAG neurons while optogenetically activating POA_{PAG} axons within the PAG. GABAergic PAG neurons were labeled by injecting AAV-FLEX-mCherry into the PAG of a VGAT-Cre mouse, while AAV-FLEXa-ChR2 was injected into the POA to express ChR2 in POA_{PAG} axon terminals within the PAG (Fig. 6A-B). After waiting four weeks to achieve functional expression of ChR2 in POA_{PAG} axon terminals, we cut brain slices from these mice and recorded optogenetically-evoked currents from fluorescently identified $VGAT^+$ PAG neurons (see Methods). Optical stimulation of POA_{PAG} axons with blue light evoked IPSCs in the majority (18/27) of voltage clamped

GABAergic PAG neurons from which we recorded (mean current=310.6 pA at 0 mV) (Fig 6C). These evoked IPSCs persisted upon application of TTX/4AP and were blocked by gabazine, indicating that POA_{PAG} axons make inhibitory synapses directly onto GABAergic PAG neurons (Fig. 6D).

To test whether these GABAergic PAG neurons synapse onto PAG-USV neurons, as predicted of a disinhibitory circuit mechanism, we injected AAV-FLEX-ChR2 into the PAG of a VGAT-Cre;TVA crossed mouse in order to express ChR2 in local $VGAT^+$ neurons (Fig. 6E). After two weeks, we used CANE (Rodriguez et al., 2017; Sakurai et al., 2016; Tschida et al., 2019) to selectively infect PAG-USV neurons with CANE-RV-mCherry (Fig. 6). Several days later, we visually targeted mCherry-expressing PAG-USV neurons for whole-cell recordings while optogenetically activating local GABAergic PAG neurons in the presence of TTX and 4AP (Fig 6F). Optogenetically activating local $VGAT^+$ neurons evoked IPSCs in almost all (13/16) of the PAG-USV neurons from which we recorded (mean current=579.9 pA at 0 mV in TTX/4AP) and these currents were completely abolished by application of gabazine (Fig 6G-H). This experiment confirms the presence of a functional connection between local inhibitory neurons and PAG-USV neurons. Taken together, these findings support a model in which activity in POA_{PAG} neurons disinhibits PAG-USV neurons, promoting the production of USVs.

Discussion

Here we used a combination of monosynaptic rabies tracing, optogenetic manipulations of neural activity in freely behaving animals, and optogenetics-assisted circuit mapping in brain slices to elucidate the functional relevance and synaptic organization of descending inputs to the PAG vocal gating circuit. We identified two populations of forebrain inhibitory neurons, one located in the POA and the other in the EA, that drive opposing effects on vocal behavior.

Optogenetic activation of POA_{PAG} neurons drives robust and long-lasting bouts of vocalization in the absence of any social cues normally required to elicit vocalizations, and the acoustic features of these “opto-USVs” shared many features with spontaneously produced social USVs. In contrast, optogenetic activation of a $VGAT^+$ population of EA_{PAG} neurons transiently suppressed USV production in male mice during active courtship without disrupting other non-vocal courtship behaviors. Further, activation of EA_{PAG} neurons did not elicit fearful or aversive behavior, indicating that the effect on vocal behavior was not driven or accompanied by a generalized change in behavioral state. Finally, we paired optogenetic activation of descending POA or EA inputs to the PAG with whole-cell recordings from PAG-USV or GABAergic PAG neurons to investigate how these POA and EA inputs drive opposing effects on vocal behavior. These slice experiments support a model in which EA_{PAG} neurons directly inhibit PAG-USV neurons to suppress vocalization, while POA_{PAG} neurons directly inhibit GABAergic PAG interneurons, which in turn inhibit PAG-USV neurons, resulting in a net disinhibition of PAG-USV neurons that promotes vocalization.

We observed that activation of POA_{PAG} neurons using a variety of viral strategies readily elicits USV production in both male and female mice (Fig. 2), in agreement with a recent report that activation of GABAergic POA neurons elicits USVs in both sexes (Gao et al., 2019). These findings contrast with the behavioral observation that female mice in general produce fewer USVs than males. For example, female mice produce only about 1/5 of the total USVs recorded during male-female courtship interactions (Neunuebel et al., 2015), and we observed that female mice vocalize at lower rates than males when encountering novel female social partners (data not shown). Taken together, these findings suggest that differential gating of POA_{PAG} activity in males and females might contribute to sex differences in vocal behavior, but that when directly activated, POA_{PAG} neurons in males and females do not differ in their ability to activate the downstream PAG vocal gating circuit. Although it remains unknown which factors

might drive differential activation of male and female POA_{PAG} neurons, it is possible that sex differences in the density (Campi et al., 2013; Gorski et al., 1978; Orikasa and Sakuma, 2010; Panzica et al., 1996), synaptic organization (Raisman and Field, 1971), and gene expression patterns (Moffitt et al., 2018; Xu et al., 2012) of POA neurons might all contribute to this sexually dimorphic behavior. More broadly, our findings add to a growing body of literature indicating that male and female brains contain latent circuits for sex-typical behaviors that can be unmasked by artificial neural activation but that are gated in a sex-specific manner during natural behavior (Clyne and Miesenbock, 2008; Gao et al., 2019; Rezaval et al., 2016; Wei et al., 2018).

Although a previous study reported that activation of $Esr1^+$ POA neurons promotes mounting (Wei et al., 2018), we failed to observe mounting when we optogenetically activated either POA_{PAG} neurons or $Esr1^+$ POA neurons in male and female mice. Although the reasons for this discrepancy remain uncertain, one possibility is that our use of lower intensity optical stimulation can account for this difference (3-5 mW, 10-20 Hz vs. 10mW, 40 Hz in Wei et al., 2018), and that the level of $Esr1^+$ POA neuronal activation required to elicit USV production is lower than the threshold to elicit mounting. An interesting possibility is that different projection-defined subsets of $Esr1^+$ POA neurons contribute to distinct aspects of courtship behavior, similar to what has been described for the contribution of projection-defined subsets of galanin-expressing POA neurons to distinct aspects of parental behavior (Kohl et al., 2018; Wu et al., 2014). Notably, though, a recent study found that ablation of $VGAT^+$ POA neurons did not affect the numbers of social USVs produced by male and female mice, although the acoustic features of male courtship USVs were altered following ablation of these neurons (Gao et al., 2019). In contrast, ablation or silencing of POA neurons greatly reduces non-vocal consummatory courtship behaviors including mounting and ejaculation (Bean et al., 1981; Floody, 1989; Wei et al., 2018). These findings are consistent with the idea that POA_{PAG} neurons promote the production of USVs during later stages of courtship (Gao et al., 2019), which differ acoustically from USVs

produced in earlier phases of courtship (Hanson and Hurley, 2012; Keesom et al., 2017; Matsumoto and Okanoya, 2016; White et al., 1998), and that other neuronal populations that lie upstream of the PAG vocal gating circuit, and that are potentially interconnected with the POA, serve to promote USV production during the early phases of courtship and in other behavioral contexts.

Here we employ a newly described VAE-based unsupervised modeling method to compare the acoustic features of optogenetically-elicited USVs to each animal's repertoire of female-directed USVs. Interestingly, although synchronous optogenetic activation of POA_{PAG} neurons is likely quite different from the natural activity patterns of these neurons, the majority of optogenetically-elicited vocalizations fall within the distribution of naturally produced USVs. This finding provides further experimental support for a model in which the PAG-USV neurons that are disinhibited by input from the POA gate USV production but do not directly pattern the acoustic content of vocalizations. The VAE also allowed us to identify and interrogate the acoustic features of optogenetically-elicited vocalizations that fell outside the natural acoustic distribution. We found that these unusual "opto-USVs" were louder and higher in frequency bandwidth, which we speculate may arise because synchronous optogenetic activation of POA neurons can, in some cases, activate the PAG vocal gating circuit more strongly than occurs during natural behavior.

The current study also identifies a novel population of GABAergic EA_{PAG} neurons that lie at a boundary zone between the central amygdala and the medial amygdala. Although this pocket of cells remains to be characterized comprehensively at a molecular and physiological level, our data show that transiently activating these neurons transiently suppresses vocal production without driving fearful or aversive responses. Additionally, optogenetically activating EA_{PAG} neurons suppresses vocalization without interrupting non-vocal courtship behaviors more generally, providing additional support for the idea that PAG-USV cells are specialized neurons that gate USV production but that do not control non-vocal aspects of courtship. Although it is

unknown whether EA_{PAG} neurons are similarly engaged in female mice who vocalize less readily than males, we identified EA_{PAG} neurons in female mice that have similar axonal projections to those observed in males (Fig. S5 and data not shown) and speculate that these neurons also inhibit USV production via direct inhibition of PAG-USV neurons.

We found that EA_{PAG} neurons make inhibitory synapses on PAG-USV neurons, which in turn gate vocalizations by exciting downstream vocal-respiratory pattern generating circuits (Tschida et al., 2019). Thus, the EA to PAG pathway provides a monosynaptic substrate through which vocalizations can be rapidly and effectively suppressed. We anticipate that such descending inhibitory inputs onto PAG-USV neurons act rapidly to suppress vocalization in behavioral contexts (in the presence of predators, conspecific competitors, etc.) in which vocalization is risky or otherwise adverse, although this idea remains to be tested. Although POA_{PAG} neurons are also GABAergic, we found that optogenetically activating these neurons promotes rather than suppresses USV production, likely through a disynaptic disinhibition of PAG-USV neurons mediated by local PAG interneurons. Consistent with the idea that disinhibition within the PAG is important for vocal production, work in primates has shown that pharmacological blockade of GABA receptors lowers the threshold for vocalization and elicits spontaneous vocalizations as well (Forcelli et al., 2017; Jurgens, 1994; Lu and Jurgens, 1993). Indeed, disinhibition of glutamatergic projection neurons has emerged as a prominent circuit motif within the PAG for releasing a variety of behaviors, including freezing (Tovote et al., 2016), pup grooming (Kohl et al., 2018), and antinociception (Morgan and Clayton, 2005). Our results support a model in which PAG-USV neuronal activity is tightly regulated by descending inputs as well as inputs from local GABAergic PAG neurons, which in turn integrate a variety of behaviorally relevant forebrain inputs to appropriately gate PAG-USV activity and hence USV production. More generally, such disinhibitory circuit motifs in the PAG may provide a failsafe mechanism that

carefully regulates the behavioral contexts in which crucial but potentially costly behaviors, including vocalizations, are produced.

By exploiting selective genetic access to PAG-USV neurons as a point of entry into central circuits for social and courtship vocalizations, we have begun to map the brain-wide architecture and synaptic organization of circuitry for a complex, natural behavior. In addition to the inputs from the POA and EA that were the focus of this study, our transsynaptic tracing identified a number of forebrain regions whose projections converge onto the PAG vocal gating circuit, consistent with the idea that the PAG integrates a wide variety of social, environmental, and internal state-related information to gate vocalization in a context-appropriate manner. Given that context-dependent vocal gating is a hallmark of human vocalizations, including speech, it will be of great interest in future studies to more fully describe the neuronal populations whose inputs to the PAG shape vocal behavior. We note that vocal behavior isn't binary, and that in addition to deciding whether or not to vocalize, an animal must produce the acoustic category of vocalization that is appropriate for a given behavioral context. The elucidation of circuit and synaptic mechanisms through which forebrain inputs to the PAG vocal gating circuit influence USV production represents an important first step toward understanding how descending forebrain neurons act on midbrain vocal gating circuits to regulate the production of acoustically distinct categories of vocalizations that differ in their communicative significance.

Materials and Methods

CONTACT FOR REAGENT AND RESOURCE SHARING

Further information and requests for resources and reagents should be directed to the Lead Contact, Richard Mooney (mooney@neuro.duke.edu).

EXPERIMENTAL MODELS AND SUBJECT DETAILS

Animal statement. All experiments were conducted according to protocols approved by the Duke University Institutional Animal Care and Use Committee.

Animals. For optogenetic activation and axonal tracing experiments, the following mouse lines from Jackson labs were used: C57 (000664), Esr1-Cre (017911), VGAT-Cre (016962), Ai14 (007908). Fos-dsTVA mice (Jackson Labs, 027831) were used for activity-dependent labeling of PAG-USV neurons employed in the transsynaptic tracing experiments and in whole-cell recording experiments. In a subset of whole-cell recording experiments, VGAT-Cre homozygous mice were crossed to Fos-dsTVA homozygous mice.

METHOD DETAILS

Viruses: The following viruses and injection volumes were used: AAV2/1-hSyn-FLEX-ChR2-eYFP (Addgene), AAV-pgk-retro-Cre (Addgene), AAV-hsyn-retro-FLEX-ChR2 (Addgene), AAV-FLEX-GFP (Addgene), AAV-FLEX-tdTomato (Addgene), AAV-FLEX-oG (Duke Viral Vector Core). EnvA-ΔG-RV-GFP, CANE-RV-mCherry, and AAV-FLEX-TVA-mCherry were produced in house as previously described (Rodriguez et al., 2017; Sakurai et al., 2016; Tschida et al., 2019). The final injection coordinates were as follows: POA, AP=0.14 mm, ML= 0.3 mm, DV= 5.5 mm; EA, AP=-1.5 mm, ML= 2.3 mm, DV= 4.6 mm; PAG, AP=-4.7 mm, ML= 0.7 mm, DV= 1.75 mm. Viruses were pressure-injected with a Nanoject II (Drummond) at a rate of 4.6 nL every 15s.

Transsynaptic tracing from PAG-USV and GABAergic PAG neurons: To selectively infect PAG-USV neurons with viruses, ds-Fos-TVA males were given social experience with a female (30-60 mins.) that resulted in high levels of USV production (500-5000 USVs total). Males were then anesthetized (1.5-2% isoflurane), and the caudolateral PAG was targeted for viral injection. For transsynaptic tracing from PAG-USV neurons, the PAG was injected with a 4:1:1 mixture of CANE-LV-Cre, AAV-FLEX-TVA-mCherry, and AAV-FLEX-oG (total volume of 300 nL). After a wait time of 10-14 days, the PAG was then injected with EnvA-ΔG-RV-GFP (100 nL, diluted 1:5), and animals were sacrificed after waiting an additional 4-7 days.

To transsynaptically label inputs to GABAergic PAG neurons, the caudolateral PAG of VGAT-Cre mice was injected with a 1:1 mixture of AAV-FLEX-TVA-mCherry, and AAV-FLEX-oG (total volume of 100 nL). After a wait time of 10-14 days, the PAG was then injected with EnvA-ΔG-RV-GFP (100 nL, diluted 1:5), and animals were sacrificed after waiting an additional 4-7 days.

In vivo optogenetic stimulation: Custom-made or commercially available (RWD) optogenetic ferrules were implanted in the same surgeries as viral injection just above target brain locations and were fixed to the skull using Metabond (Parkell). Neurons or their axon terminals were optogenetically activated with illumination from a 473 nm laser (3-15 mW) at 10-20 Hz (50 ms pulses, 2-10s total) or with phasic laser pulses (1-2s duration). Laser stimuli were driven by computer-controlled voltage pulses (Spike 7, CED).

Post-hoc visualization of viral labeling: Mice were deeply anaesthetized with isoflurane and then transcardially perfused with ice-cold 4% paraformaldehyde in 0.1 M phosphate buffer, pH 7.4 (4% PFA). Dissected brain samples were post-fixed overnight in 4% PFA at 4 °C, cryoprotected in a 30% sucrose solution in PBS at 4 °C for 48 hours, frozen in Tissue-Tek O.C.T. Compound (Sakura), and stored at –80 °C until sectioning. To visualize viral labeling post-hoc, brains were cut into 80 µm coronal sections, rinsed 3x in PBS, and processed for 24 hours at 4 degrees with NeuroTrace (1:500 Invitrogen) in PBS containing 0.3% Triton-X. Tissue

sections rinsed again 3 x 10 mins. in PBS, mounted on slides, and coverslipped with Fluoromount-G (Southern Biotech). After drying, slides were imaged with a 10x objective on a Zeiss 700 laser scanning confocal microscope.

Floating section two-color in situ hybridization: In situ hybridization was performed using hybridization chain reaction (HCR v3.0, Molecular Instruments). Dissected brain samples were post-fixed overnight in 4% PFA at 4 °C, cryoprotected in a 30% sucrose solution in RNAse-free PBS (i.e., DEPC-PBS) at 4 °C for 48 hours, frozen in Tissue-Tek O.C.T. Compound (Sakura), and stored at –80 °C until sectioning. 80-µm thick coronal floating sections were collected into a sterile 24 well plate in DEPC-PBS, fixed again briefly for 5 min. in 4% PFA, then placed in 70% EtOH in DEPC-PBS overnight. Sections were rinsed in DEPC-PBS, incubated for 45 min in 5% SDS in DEPC-PBS, rinsed and incubated in 2x SSCT, pre-incubated in HCR hybridization buffer at 37 °C, and then placed in HCR hybridization buffer containing RNA probes overnight at 37 °C. The next day, sections were rinsed 4 x 15 minutes at 37 °C in HCR probe wash buffer, rinsed with 2X SSCT, pre-incubated with HCR amplification buffer, then incubated in HCR amplification buffer containing HCR amplifiers at room temperature for ~48 hours. On the final day, sections were rinsed in 2x SSCT, counterstained with DAPI (Thermo Fisher, 1:5000), rinsed again with 2x SSCT, then mounted on slides and coverslipped with Fluoromount-G (Southern Biotech). After drying, slides were imaged with a 10x or 20x objective on a Zeiss 700 laser scanning confocal microscope.

USV recording and analysis. To elicit USVs, single-housed males or females were presented with a freely moving female, either in a novel test chamber or in the home cage. USVs were recorded with an ultrasonic microphone (Avisoft, CMPA/CM16), amplified (Presonus TubePreV2), and digitized at 250 kHz (Spike 7, CED). USVs were detected using codes from the Holy lab (http://holylab.wustl.edu/) using the following parameters (mean frequency > 45 kHz; spectral purity > 0.3; spectral discontinuity < 0.85; min. USV duration = 5 ms; minimum

inter-syllable interval = 30 ms). To elicit USVs for tagging of PAG-USV neurons using CANE (for transsynaptic tracing and slice experiments), Fos^{TVA} males were given social experience with a female (30-60 min. session), either in their home cage fitted with an acoustically permeable lid or in a test chamber that had no lid and allowed easy microphone access. Sixty minutes from the start of the session, Fos^{TVA} males were anesthetized and taken for injection of the PAG with viruses (see above), such that injections began approximately 2 hours from the start of USV production.

Real-time place preference tests: Mice were lightly anesthetized to connect the 473 nm laser to the optogenetic ferrule, then mice were placed in the center of a custom-made two-sided test chamber, illuminated with infrared light only. The side of the chamber in which each mouse received optogenetic stimulation was chosen randomly for each place preference test. When the mouse was in the selected side, it received continuous 10 Hz optogenetic stimulation using the minimum laser power that had either elicited or inhibited USV production for that same mouse. Place preference was scored over a 20 minute test period as the proportion of the total time that the mouse spent in the stimulated side of the chamber.

Quantification of optogenetically-elicited body movements: The mouse's position was measured using custom Matlab codes that detected and tracked the centroid of the mouse's body position across video frames (Logitech webcam, 30 frames per second), and speed of movement was calculated as the change in position across pairs of frames. To align movement with optogenetic activation of POA or EA neurons, we first estimated the temporal offset between the webcam video and USV audio by calculating the time of the peak cross-covariance between the high-pass filtered webcam audio and the low-pass filtered USV audio. This offset was then used to align the mouse's movement to the onset of each optogenetic laser stimulus. To measure the effects of optogenetic stimulation on the distance between an interacting male and female mouse, the position of each mouse was tracked manually in every 6th frame, and the

distance between mice was scored as the distance from the center of the male's head to the base of the female's tail.

Comparison of acoustic features of optogenetically-elicited USVs to female-directed USVs: 52,821 USV syllables were segmented automatically with MUPET 2.0 using default parameter settings (Van Segbroeck et al., 2017). 23,805 of these syllables came from recordings of 15 mice recorded under both natural and optogenetic conditions (56% natural USVs). The remaining 29,016 syllables came from recordings of a control group of 10 mice used to establish across-day syllable repertoire variability. False positives (noise) from the experimental group were manually removed by visual inspection of spectrograms, with 79% of the original syllables retained. Syllables were analyzed using Autoencoded Vocal Analysis v0.2 (Goffinet, 2019), a Python package for generating low-dimensional latent descriptions of animal vocalizations using a variational autoencoder (VAE) (Kingma, 2013). Briefly, the VAE jointly trains two probabilistic maps: an encoder and a decoder. Spectrograms are encoded into low-dimensional "latent" representations which can be subsequently decoded to approximately reconstruct the original spectrograms. Both encoding and decoding distributions are parameterized by convolutional neural networks. We trained a VAE on spectrograms of single USV syllables from both experimental and control groups using the following parameters: min_freq=30e3, max_freq=110e3, nperseg=1024, noverlap=512, spec_min_val=-5.0, spec_max_val=-1.5, mel=False, time_stretch=True, within_syll_normalize=False. Each input spectrogram was 128-by-128 pixels (16000 dimensions) and the VAE converged on a parsimonious representation of only 5 dimensions. To visualize these 5-dimensional spaces, the latent representations of syllable spectrograms are projected into two dimensions using the UMAP algorithm (McInnes, 2018). To quantify differences in syllable repertoires, we estimate the Maximum Mean Discrepancy (Gretton, 2012) between distributions of latent syllable representations as in (Goffinet, 2019). First, a baseline level of variability in syllable repertoire

was established for each mouse by estimating MMD between the first and second halves of female-directed syllables emitted in a recording session. Then MMD between each mouse's natural and optogenetically-elicited repertoires was estimated. A paired comparison test revealed significantly larger differences between optogenetic and natural repertoires than expected by variability within the natural condition recording sessions alone (two-sided, continuity-corrected Wilcoxon signed-rank test, W=9, p<5e-3). We then estimated MMD between female-directed syllable repertoires recorded on different days, using the set of 10 control mice.

Whole-cell recordings: Mice that received viral injections 2-4 weeks prior were deeply anesthetized with isoflurane and standard procedures were used to prepare 300 µm thick coronal slices. The brain was dissected in ice-cold ACSF containing the following (in mM): 119 NaCl, 2.5 KCl, 1.30 $MgCl_2$, 2.5 $CaCl_2$, 26.2 $NaHCO_3$, 1.0 $NaHPO_4$-H_2O, and 11.0 dextrose and bubbled with 95% O_2/5% CO_2. The brain was mounted on an agar block and sliced in ice-cold ACSF with a vibrating-blade microtome (Leica). Slices were incubated for 15 minutes at 32ºC in a bath of NMDG recovery solution containing the following (in mM): 93.0 NMDG, 2.5 KCl, 1.2 NaH_2PO_4, 30.0 $NaHCO_3$, 20.0 HEPES, 25.0 glucose, 2.0 thiourea, 5.0 Na L-ascorbate, 2.0 Na-pyruvate, 10.0 $MgSO_4$ $7H_2O$, 0.5 $CaCl_2$, and 95.0 HCl. Slices were then moved to a bath of HEPES storage solution containing the following (in mM): 93.0 NaCl, 2.5 KCl, 1.2 NaH_2PO_4, 30.0 $NaHCO_3$, 20.0 HEPES, 25.0 glucose, 2.0 thiourea, 5.0 Na L-ascorbate, 2.0 Na-pyruvate, 10.0 $MgSO_4$ $7H_2O$, and 0.5 $CaCl_2$, and allowed to gradually reach room temperature over the course of 1 hour, where they remained for the duration. Recordings were performed in ACSF at a temperature of 32ºC. For voltage clamp experiments patch electrodes (4-8 MΩ) were filled with cesium internal solution containing the following (in mM): 130 cesium methanesulfonate, 5 QX-314 Br, 10 HEPES, 8 TEA-Cl, 0.2 EGTA, 4 ATP-Mg salt, 0.3 GTP-Na salt, and 10 phosphocreatine. Recordings were made using a Multiclamp 700B amplifier whose output was

digitized at 10 kHz (Digidata 1440A). Series resistance was <25 MΩ and was compensated up to 90%. Signals were analyzed using Igor Pro (Wavemetrics). Neurons were targeted using interference contrast and epifluorescence to visualize fluorescent indicators previously expressed via viral injection. ChR2-expressing axon terminals were stimulated by 5-20 ms laser pulses (3-10 mW) from a 473 nm laser delivered via fiber optic inside the recording pipette (Optopatcher, A-M Systems). To confirm the direct nature of optogenetically evoked currents 2µM TTX (Tocris) and 100µM 4AP (Sigma-Aldrich) were added to the ACSF and perfused onto slices. To confirm that evoked currents were GABAergic, 10µM gabazine (Tocris) was applied. Pharmacological agents including were bath applied for 10 minutes before making recordings.

Data availability: The data that support the findings of this study are available from the corresponding author upon reasonable request.

Code availability: All custom-written Matlab codes used in this study are available from the corresponding author. The latest version of Autoencoded Vocal Analysis, the Python package used to generate, plot, and analyze latent features of mouse USVs, is freely available online: https://github.com/jackgoffinet/autoencoded-vocal-analysis.

QUANTIFICATION AND STATISTICAL ANALYSES

Statistics: Parametric, two-sided statistical comparisons were used in all analyses unless otherwise noted (alpha=0.05). No statistical methods were used to predetermine sample sizes. Error bars represent standard error of the mean unless otherwise noted.

Acknowledgements: Thanks to Michael Booze and Bao-Xia Han for additional mouse husbandry, thanks to Jun Takatoh for help with HCR in situ hybridization, and thanks to Shengli Zhao for providing CANE-related viruses. This work is supported by NIH grants DC 013826 (to R.M.) and MH 117778 (to F.W. and R.M.).

Author contributions: VM, KAT, JP, FW, and RM designed the experiments. VM and KAT conducted the experiments. VM, KAT, and JG analyzed data. VM, KAT, and RM wrote the manuscript, and all authors approved the final manuscript.

Competing interests: The authors declare no competing interests.

References

Alger, S.J., and Riters, L.V. (2006). Lesions to the medial preoptic nucleus differentially affect singing and nest box-directed behaviors within and outside of the breeding season in European starlings (Sturnus vulgaris). Behav Neurosci *120*, 1326-1336.

Balthazart, J., and Ball, G.F. (2007). Topography in the preoptic region: differential regulation of appetitive and consummatory male sexual behaviors. Front Neuroendocrinol *28*, 161-178.

Bandler, R., and Shipley, M.T. (1994). Columnar organization in the midbrain periaqueductal gray: modules for emotional expression? Trends Neurosci *17*, 379-389.

Bean, N.Y., Nunez, A.A., and Conner, R. (1981). Effects of medial preoptic lesions on male mouse ultrasonic vocalizations and copulatory behavior. Brain Res Bull *6*, 109-112.

Bennett, P.J.G., Maier, E., and Brecht, M. (2019). Involvement of rat posterior prelimbic and cingulate area 2 in vocalization control. Eur J Neurosci *50*, 3164-3180.

Campi, K.L., Jameson, C.E., and Trainor, B.C. (2013). Sexual Dimorphism in the Brain of the Monogamous California Mouse (Peromyscus californicus). Brain Behav Evol *81*, 236-249.

Carrive, P. (1993). The periaqueductal gray and defensive behavior: functional representation and neuronal organization. Behav Brain Res *58*, 27-47.

Chabout, J., Sarkar, A., Dunson, D.B., and Jarvis, E.D. (2015). Male mice song syntax depends on social contexts and influences female preferences. Front Behav Neurosci *9*, 76.

Clyne, J.D., and Miesenbock, G. (2008). Sex-specific control and tuning of the pattern generator for courtship song in Drosophila. Cell *133*, 354-363.

Dujardin, E., and Jurgens, U. (2006). Call type-specific differences in vocalization-related afferents to the periaqueductal gray of squirrel monkeys (Saimiri sciureus). Behav Brain Res *168*, 23-36.

Duvarci, S., and Pare, D. (2014). Amygdala microcircuits controlling learned fear. Neuron *82*, 966-980.

Ehrlich, I., Humeau, Y., Grenier, F., Ciocchi, S., Herry, C., and Luthi, A. (2009). Amygdala inhibitory circuits and the control of fear memory. Neuron *62*, 757-771.

Evans, D.A., Stempel, A.V., Vale, R., Ruehle, S., Lefler, Y., and Branco, T. (2018). A synaptic threshold mechanism for computing escape decisions. Nature *558*, 590-594.

Fang, Y.Y., Yamaguchi, T., Song, S.C., Tritsch, N.X., and Lin, D. (2018). A Hypothalamic Midbrain Pathway Essential for Driving Maternal Behaviors. Neuron *98*, 192-207 e110.

Floody, O.R. (1989). Dissociation of hypothalamic effects on ultrasound production and copulation. Physiol Behav *46*, 299-307.

Floody, O.R. (2009). Effects on hamster vocalization and aggression of carbachol injections into the MPOA/AH. Physiol Behav *96*, 294-299.

Floody, O.R., Cooper, T.T., and Albers, H.E. (1998). Injection of oxytocin into the medial preoptic-anterior hypothalamus increases ultrasound production by female hamsters. Peptides *19*, 833-839.

Forcelli, P.A., Waguespack, H.F., and Malkova, L. (2017). Defensive Vocalizations and Motor Asymmetry Triggered by Disinhibition of the Periaqueductal Gray in Non-human Primates. Front Neurosci *11*, 163.

Fu, X.W., and Brudzynski, S.M. (1994). High-frequency ultrasonic vocalization induced by intracerebral glutamate in rats. Pharmacol Biochem Behav *49*, 835-841.

Gao, S.C., Wei, Y.C., Wang, S.R., and Xu, X.H. (2019). Medial Preoptic Area Modulates Courtship Ultrasonic Vocalization in Adult Male Mice. Neurosci Bull *35*, 697-708.

Goffinet, J., Mooney, R., Pearson, J. (2019). Inferring low-dimensional latent descriptions of animal vocalizations. bioRxiv.

Gorski, R.A., Gordon, J.H., Shryne, J.E., and Southam, A.M. (1978). Evidence for a morphological sex difference within the medial preoptic area of the rat brain. Brain Res *148*, 333-346.
Green, D.B., Shackleton, T.M., Grimsley, J.M.S., Zobay, O., Palmer, A.R., and Wallace, M.N. (2018). Communication calls produced by electrical stimulation of four structures in the guinea pig brain. PLoS One *13*, e0194091.
Gretton, A., Borgwardt, K.M., Rasch, M.J., Scholkopf, B., Smola, A. (2012). A Kernel Two-Sample Test. Journal of Machine Learning Research *13*, 723-773.
Hanson, J.L., and Hurley, L.M. (2012). Female presence and estrous state influence mouse ultrasonic courtship vocalizations. PLoS One *7*, e40782.
Holstege, G. (2014). The periaqueductal gray controls brainstem emotional motor systems including respiration. Prog Brain Res *209*, 379-405.
Holy, T.E., and Guo, Z. (2005). Ultrasonic songs of male mice. PLoS Biol *3*, e386.
Janak, P.H., and Tye, K.M. (2015). From circuits to behaviour in the amygdala. Nature *517*, 284-292.
Jurgens, U. (1982). Amygdalar vocalization pathways in the squirrel monkey. Brain Res *241*, 189-196.
Jurgens, U. (1994). The role of the periaqueductal grey in vocal behaviour. Behav Brain Res *62*, 107-117.
Jurgens, U. (2002). Neural pathways underlying vocal control. Neurosci Biobehav Rev *26*, 235-258.
Jurgens, U. (2009). The neural control of vocalization in mammals: a review. J Voice *23*, 1-10.
Jurgens, U., and Ploog, D. (1970). Cerebral representation of vocalization in the squirrel monkey. Exp Brain Res *10*, 532-554.
Jurgens, U., and Pratt, R. (1979). Role of the periaqueductal grey in vocal expression of emotion. Brain Res *167*, 367-378.
Jurgens, U., and Richter, K. (1986). Glutamate-induced vocalization in the squirrel monkey. Brain Res *373*, 349-358.
Keesom, S.M., Finton, C.J., Sell, G.L., and Hurley, L.M. (2017). Early-Life Social Isolation Influences Mouse Ultrasonic Vocalizations during Male-Male Social Encounters. PLoS One *12*, e0169705.
Kingma, D.P., Welling, M. (2013). Auto-Encoding Variational Bayes. ArXiv.
Kohl, J., Babayan, B.M., Rubinstein, N.D., Autry, A.E., Marin-Rodriguez, B., Kapoor, V., Miyamishi, K., Zweifel, L.S., Luo, L., Uchida, N.*, et al.* (2018). Functional circuit architecture underlying parental behaviour. Nature *556*, 326-331.
Kyuhou, S., and Gemba, H. (1998). Two vocalization-related subregions in the midbrain periaqueductal gray of the guinea pig. Neuroreport *9*, 1607-1610.
LeDoux, J. (2007). The amygdala. Curr Biol *17*, R868-874.
Lu, C.L., and Jurgens, U. (1993). Effects of chemical stimulation in the periaqueductal gray on vocalization in the squirrel monkey. Brain Res Bull *32*, 143-151.
Ma, J., and Kanwal, J.S. (2014). Stimulation of the basal and central amygdala in the mustached bat triggers echolocation and agonistic vocalizations within multimodal output. Front Physiol *5*, 55.
Maggio, J.C., and Whitney, G. (1985). Ultrasonic vocalizing by adult female mice (Mus musculus). J Comp Psychol *99*, 420-436.
Manteuffel, G., Schon, P.C., Dupjan, S., Tuchscherer, A., and Bellmann, O. (2007). Acetylcholine injection into the amygdala elicits vocalization in domestic pigs (Sus scrofa). Behav Brain Res *178*, 177-180.
Matsumoto, Y.K., and Okanoya, K. (2016). Phase-Specific Vocalizations of Male Mice at the Initial Encounter during the Courtship Sequence. PLoS One *11*, e0147102.

McInnes, L., Healy, J., Melville, J. (2018). UMAP: Uniform Manifold Approximation and Projection for Dimension Reduction. arXiv.
McKinsey, G., Ahmed, O.M., and Shah, N.M. (2018). Neural control of sexually dimorphic social behaviors. Curr Opin Physiol *6*, 89-95.
Moffitt, J.R., Bambah-Mukku, D., Eichhorn, S.W., Vaughn, E., Shekhar, K., Perez, J.D., Rubinstein, N.D., Hao, J., Regev, A., Dulac, C.*, et al.* (2018). Molecular, spatial, and functional single-cell profiling of the hypothalamic preoptic region. Science *362*.
Morgan, M.M., and Clayton, C.C. (2005). Defensive behaviors evoked from the ventrolateral periaqueductal gray of the rat: comparison of opioid and GABA disinhibition. Behav Brain Res *164*, 61-66.
Neunuebel, J.P., Taylor, A.L., Arthur, B.J., and Egnor, S.E. (2015). Female mice ultrasonically interact with males during courtship displays. Elife *4*.
Newman, S.W. (1999). The medial extended amygdala in male reproductive behavior. A node in the mammalian social behavior network. Ann N Y Acad Sci *877*, 242-257.
Nyby, J., Wysocki, C.J., Whitney, G., Dizinno, G., and Schneider, J. (1979). Elicitation of male mouse (Mus muscululs) ultrasonic vocalization: 1. Urinary Cues. Journal of Comparative and Physiological Psychology *93*, 957-975.
Orikasa, C., and Sakuma, Y. (2010). Estrogen configures sexual dimorphism in the preoptic area of C57BL/6J and ddN strains of mice. J Comp Neurol *518*, 3618-3629.
Panzica, G.C., Viglietti-Panzica, C., and Balthazart, J. (1996). The sexually dimorphic medial preoptic nucleus of quail: a key brain area mediating steroid action on male sexual behavior. Front Neuroendocrinol *17*, 51-125.
Portfors, C.V., and Perkel, D.J. (2014). The role of ultrasonic vocalizations in mouse communication. Curr Opin Neurobiol *28*, 115-120.
Raisman, G., and Field, P.M. (1971). Sexual dimorphism in the preoptic area of the rat. Science *173*, 731-733.
Rezaval, C., Pattnaik, S., Pavlou, H.J., Nojima, T., Bruggemeier, B., D'Souza, L.A.D., Dweck, H.K.M., and Goodwin, S.F. (2016). Activation of Latent Courtship Circuitry in the Brain of Drosophila Females Induces Male-like Behaviors. Curr Biol *26*, 2508-2515.
Riters, L.V., and Ball, G.F. (1999). Lesions to the medial preoptic area affect singing in the male European starling (Sturnus vulgaris). Horm Behav *36*, 276-286.
Rodriguez, E., Sakurai, K., Xu, J., Chen, Y., Toda, K., Zhao, S., Han, B.X., Ryu, D., Yin, H., Liedtke, W.*, et al.* (2017). A craniofacial-specific monosynaptic circuit enables heightened affective pain. Nat Neurosci *20*, 1734-1743.
Sainburg, T., Theilman, B., Thielk, M., and Gentner, T.Q. (2019). Parallels in the sequential organization of birdsong and human speech. Nat Commun *10*, 3636.
Sakurai, K., Zhao, S., Takatoh, J., Rodriguez, E., Lu, J., Leavitt, A.D., Fu, M., Han, B.X., and Wang, F. (2016). Capturing and Manipulating Activated Neuronal Ensembles with CANE Delineates a Hypothalamic Social-Fear Circuit. Neuron *92*, 739-753.
Siebert, S., and Jurgens, U. (2003). Vocalization after periaqueductal grey inactivation with the GABA agonist muscimol in the squirrel monkey. Neurosci Lett *340*, 111-114.
Tovote, P., Esposito, M.S., Botta, P., Chaudun, F., Fadok, J.P., Markovic, M., Wolff, S.B., Ramakrishnan, C., Fenno, L., Deisseroth, K.*, et al.* (2016). Midbrain circuits for defensive behaviour. Nature *534*, 206-212.
Tschida, K., Michael, V., Takatoh, J., Han, B.X., Zhao, S., Sakurai, K., Mooney, R., and Wang, F. (2019). A Specialized Neural Circuit Gates Social Vocalizations in the Mouse. Neuron *103*, 459-472 e454.
Van Segbroeck, M., Knoll, A.T., Levitt, P., and Narayanan, S. (2017). MUPET-Mouse Ultrasonic Profile ExTraction: A Signal Processing Tool for Rapid and Unsupervised Analysis of Ultrasonic Vocalizations. Neuron *94*, 465-485 e465.

Vandries, L.M., Ghorbanpoor, S., Cornez, G., Shevchouk, O.T., Ball, G.F., Cornil, C.A., and Balthazart, J. (2019). Testosterone or Estradiol When Implanted in the Medial Preoptic Nucleus Trigger Short Low-Amplitude Songs in Female Canaries. eNeuro *6*.

Wei, Y.C., Wang, S.R., Jiao, Z.L., Zhang, W., Lin, J.K., Li, X.Y., Li, S.S., Zhang, X., and Xu, X.H. (2018). Medial preoptic area in mice is capable of mediating sexually dimorphic behaviors regardless of gender. Nat Commun *9*, 279.

White, N.R., Prasad, M., Barfield, R.J., and Nyby, J.G. (1998). 40- and 70-kHz vocalizations of mice (Mus musculus) during copulation. Physiol Behav *63*, 467-473.

Whitney, G., Alpern, M., Dizinno, G., and Horowitz, G. (1974). Female odors evoke ultrasounds from male mice. Anim Learn Behav *2*, 13-18.

Wu, Z., Autry, A.E., Bergan, J.F., Watabe-Uchida, M., and Dulac, C.G. (2014). Galanin neurons in the medial preoptic area govern parental behaviour. Nature *509*, 325-330.

Xu, X., Coats, J.K., Yang, C.F., Wang, A., Ahmed, O.M., Alvarado, M., Izumi, T., and Shah, N.M. (2012). Modular genetic control of sexually dimorphic behaviors. Cell *148*, 596-607.

Figure 1. Inhibitory neurons in the hypothalamus and amygdala provide input to the PAG vocal gating circuit

A Monosynaptic Inputs to PAG-USV neurons (N=4 mice)

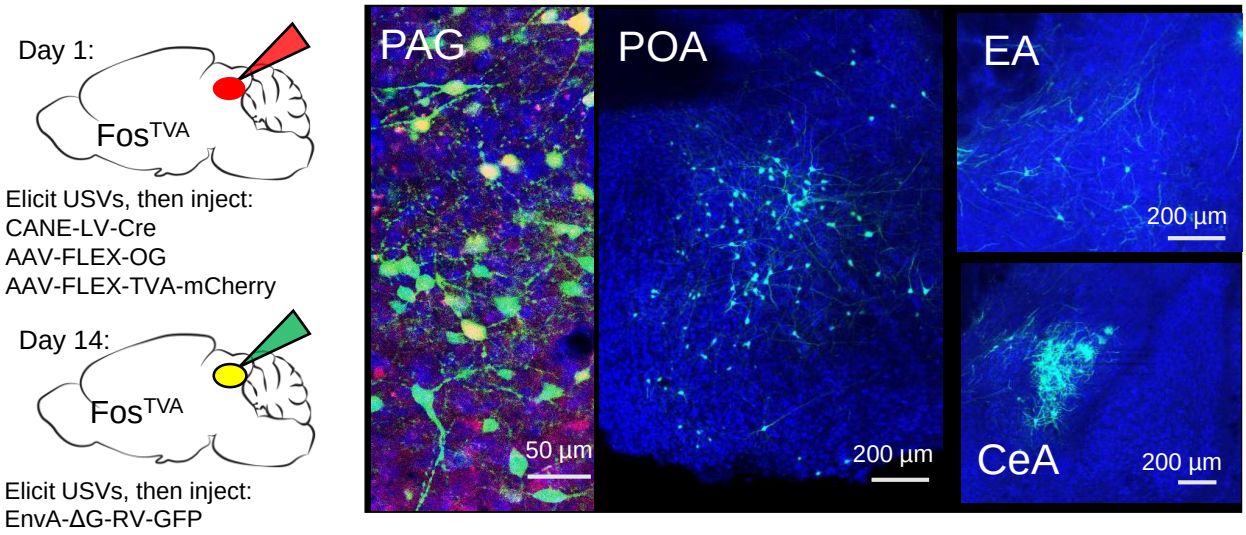

B Monosynaptic Inputs to PAG-VGAT^{+} neurons (N=6 mice)

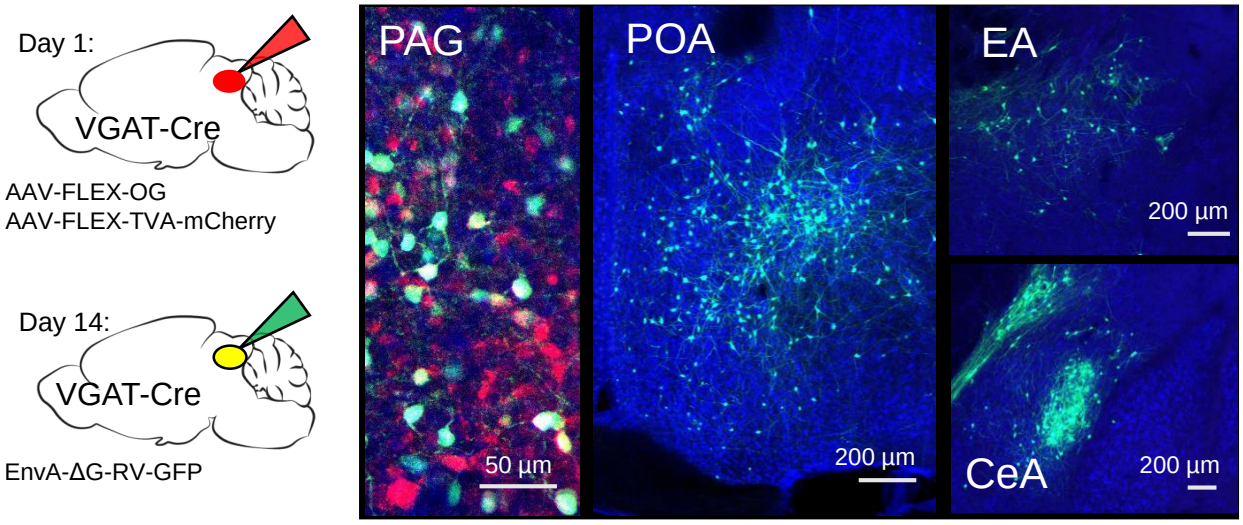

C POA inputs to PAG-VGAT^{+} neurons

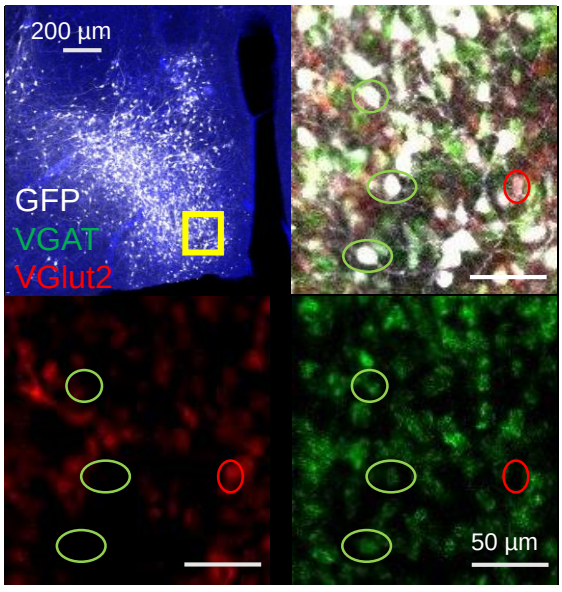

D

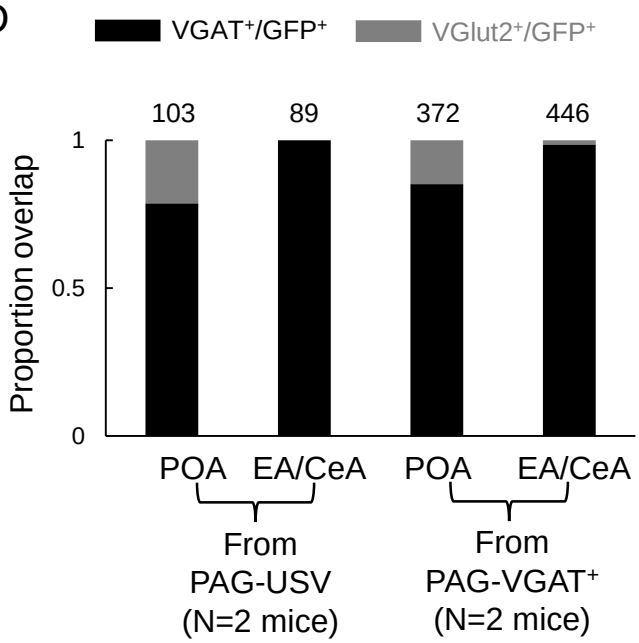

Figure 1: Inhibitory neurons in the hypothalamus and amygdala provide input to the PAG vocal gating circuit. (A) (Left) Viral strategy shown for transsynaptic labeling of direct inputs to PAG-USV neurons. (Right) Confocal images are shown of starter PAG-USV neurons, upstream neurons labeled within the POA, and upstream neurons labeled within the EA and CeA. (B) Same, for transsynaptic labeling of direct inputs to GABAergic PAG neurons. (C) Representative confocal image of in situ hybridization performed on transsynaptically-labeled POA neurons that provide direct input to GABAergic PAG neurons (labeled with GFP, shown in white), showing overlap with expression of VGAT (green) and VGlut2 (red). DAPI shown in blue. (D) Quantification of overlap of transsynaptically labeled POA and amygdala neurons with VGAT and VGlut2 (N=2 mice per condition). Total numbers of neurons scored for overlap in each condition are indicated by the numbers over the bars. See also Table S1.

Figure 2. Activating POA_{PAG} neurons elicits USVs in the absence of social cues

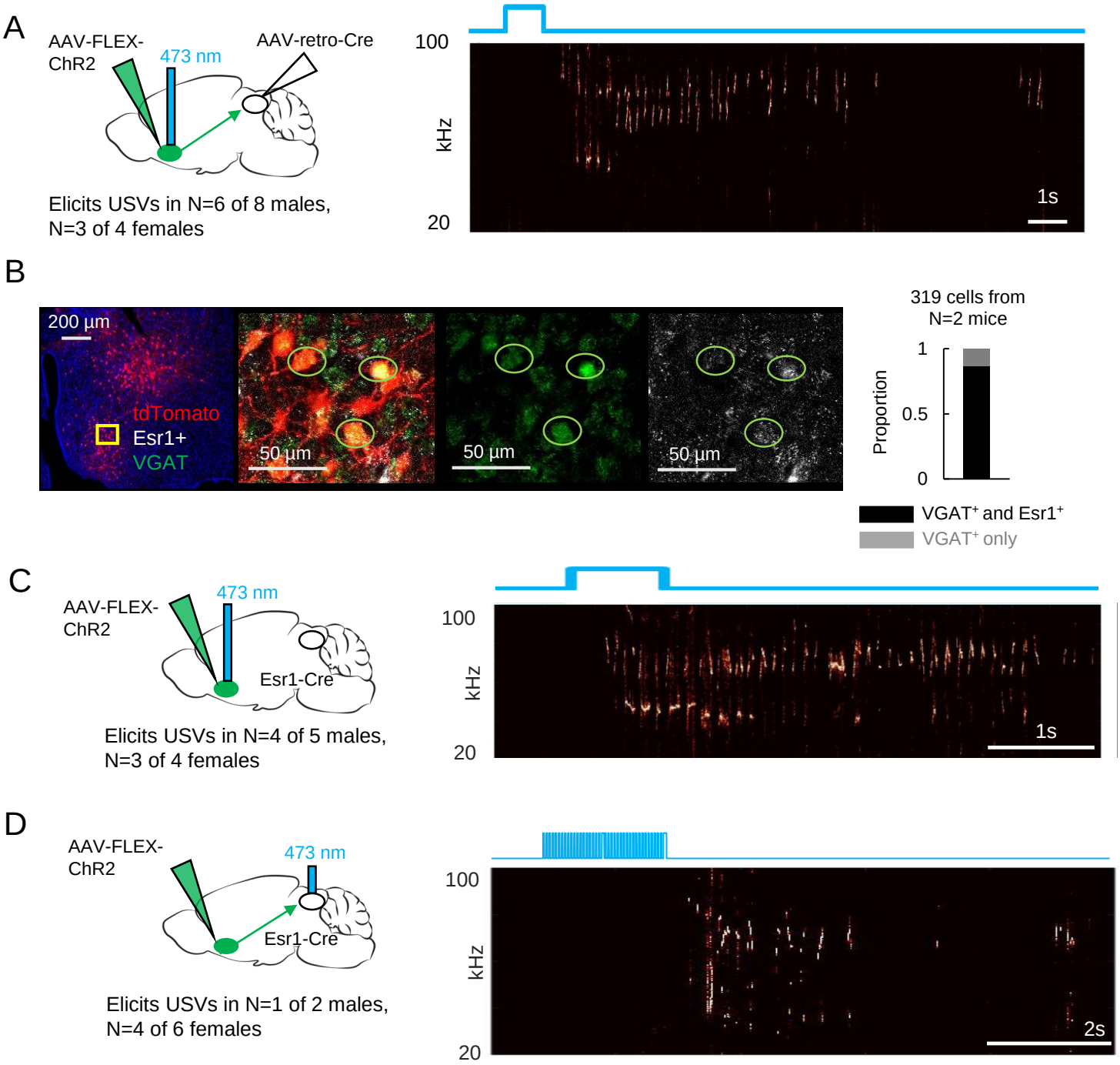

Figure 2: Activating POA_{PAG} neurons elicits USVs in the absence of social cues. (A) (Left) Viral strategy to express ChR2 in POA_{PAG} neurons. (Right) Example trial showing that optogenetic activation of POA_{PAG} neurons elicits USV production in an isolated animal. (B) Representative confocal image and quantification of in situ hybridization performed on POA_{PAG} neurons (tdTomato, red), showing overlap with Esr1 (white) and VGAT (green). DAPI is blue, N=2 mice. (C) Viral strategy used to express ChR2 in $Esr1^+$ POA neurons, and representative spectrogram of USVs that were elicited by optogenetic activation of $Esr1^+$ POA neurons. (D) Viral strategy used to optogenetically activate the axon terminals of $Esr1^+$ POA neurons within the PAG, and representative spectrogram of optogenetically-elicited USVs. See also Figures S1, S2, and S5.

Figure 3. Acoustic characterization of USVs elicited by optogenetic activation of POA neurons

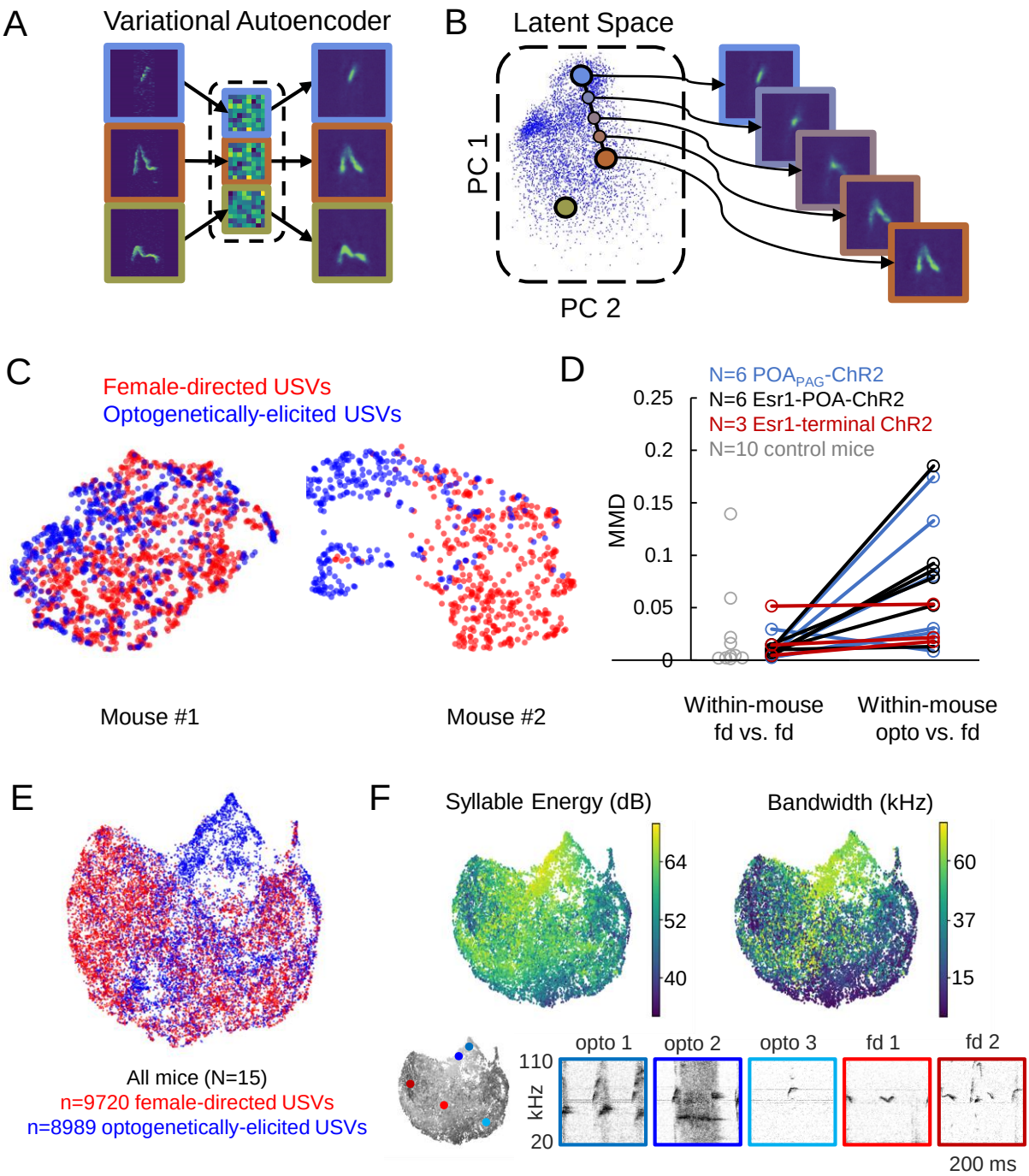

Figure 3: Acoustic characterization of USVs elicited by optogenetic activation of POA neurons. (A) The VAE takes spectrograms as input (left), maps the spectrograms to low-dimensional latent representations using an encoder (middle), and approximately reconstructs the input spectrogram using a decoder (right). (B) (Left) Dimensionality reduction techniques such as PCA or UMAP can be used to visualize the resulting latent vectors. (Right) Interpolations in latent space correspond to smooth USV syllable changes in spectrogram space exhibiting realistic dimensions of variation. (C) UMAP projections of latent syllable representations of female-directed USVs (red) and optogenetically-elicited USVs (blue) from two example mice. (D) MMD was calculated between distributions of latent syllable representations to generate three comparisons: female-directed USVs from the first half of the recording session vs. female-directed USVs from the second half, all female-directed USVs vs. opto-USVs (N=16 experimental mice), and female-directed USVs from two different recordings sessions in N=10 control mice (gray points). Note that larger MMD values indicate that distributions are more dissimilar (E) UMAP projections of latent descriptions of female-directed (red) and optogenetically-elicited USVs (blue) for all mice (N=15). (F) UMAP projections of optogenetically-elicited USVs only, color-coded by total energy (left) and frequency bandwidth (right). Example spectrograms of opto-USVS and female-directed USVs are plotted below, and the location of each example USV in UMAP space is indicated by the colored dots on the grayscale UMAP projection on the bottom left.

Figure 4: Activation of EA_{PAG} neurons transiently suppresses USV production

A

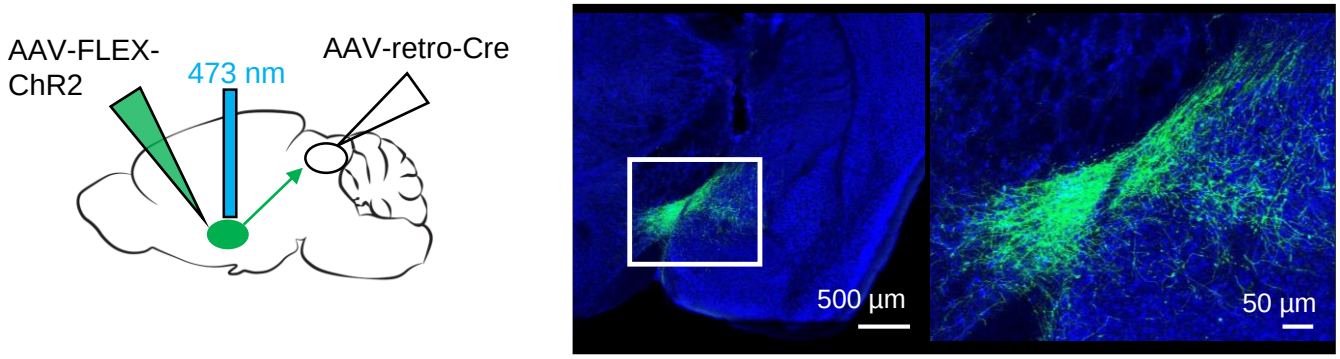

B

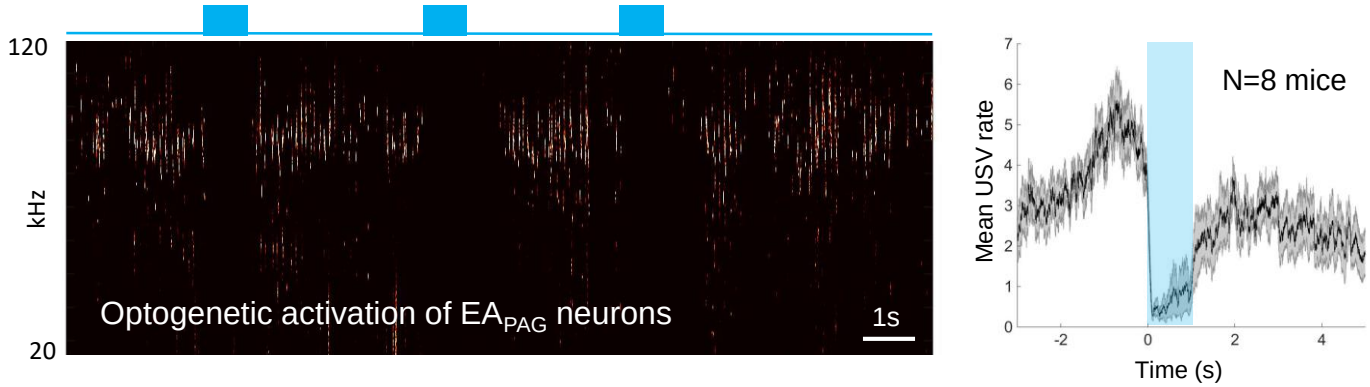

C

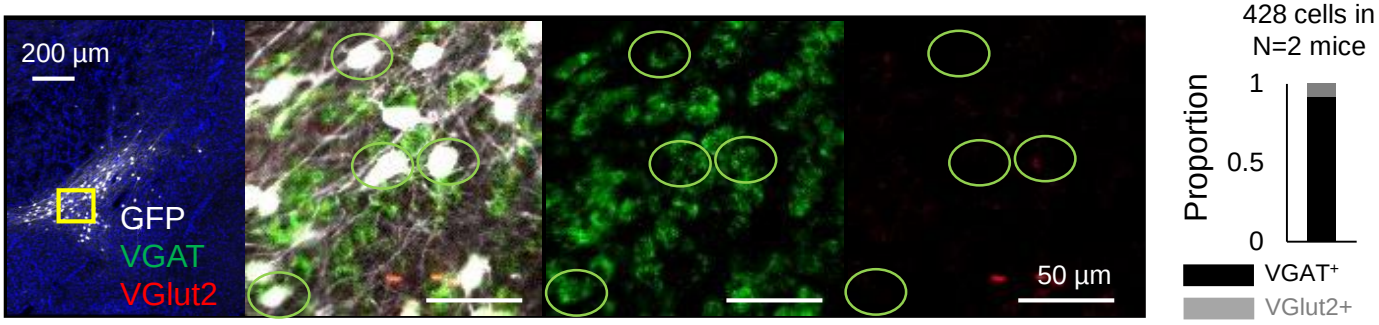

D

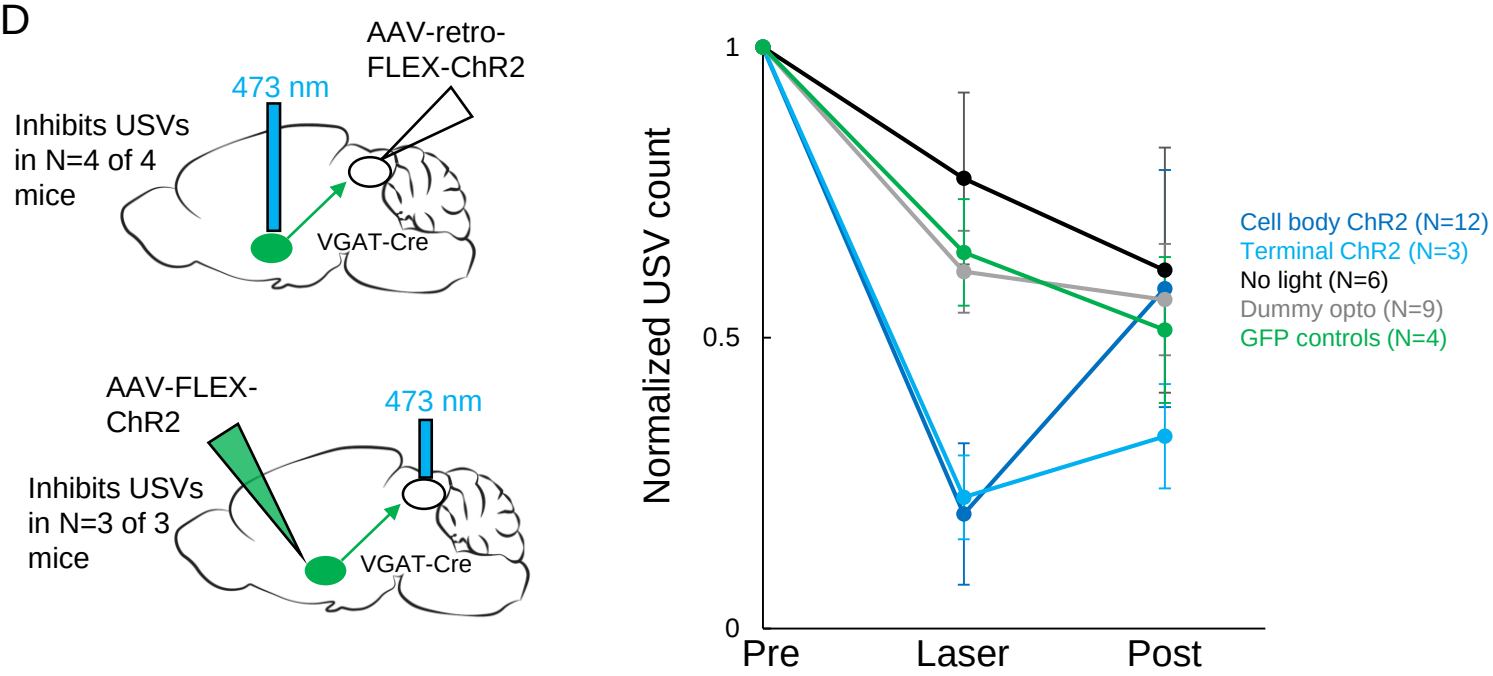

Figure 4: Activating EA_{PAG} neurons transiently suppresses USV production. (A) (Left) Viral strategy used to express ChR2 in EA_{PAG} neurons. (Right) Confocal image of representative EA_{PAG} cell body labeling achieved with this viral strategy. (B) (Left) Spectrogram showing a representative trial in which optogenetic activation of EA_{PAG} neurons suppresses USV production during the laser stimulation period. (Right) Group data quantified for N=8 mice. (C) Confocal image and quantification of in situ hybridization performed on EA_{PAG} neurons (GFP, shown in white), showing overlap with VGlut2 (red) and VGAT (green). DAPI in blue, N=2 mice. (D) Left: viral strategy used to express ChR2 in the PAG axon terminals of EA_{PAG} neurons. Right: Quantification of the number of USVs produced in the 1s period prior to optogenetic stimulation (pre), the 1s period of optogenetic stimulation (laser), and the 1s period following optogenetic stimulation (post). Data for each mouse were normalized by dividing the pre, laser, and post measurements by the total number of USVs produced during the pre-laser period. Group averages are shown for mice in which EA_{PAG} neurons were optogenetically activated (N=12, dark blue), mice in which the PAG axon terminals of EA_{PAG} neurons were optogenetically activated (N=3, light blue), control mice in which the blue laser was shined over the mouse's head but not connected to the optogenetic ferrule (N=9, gray), control mice in which GFP was expressed in EA_{PAG} neurons (N=4, green), and control mice in which the laser was triggered but not turned on (N=6, black). Error bars represent S.E.M. See also Figures S1, S3, S4, and S5.

Figure 5: EA neurons provide direct inhibition onto PAG-USV neurons

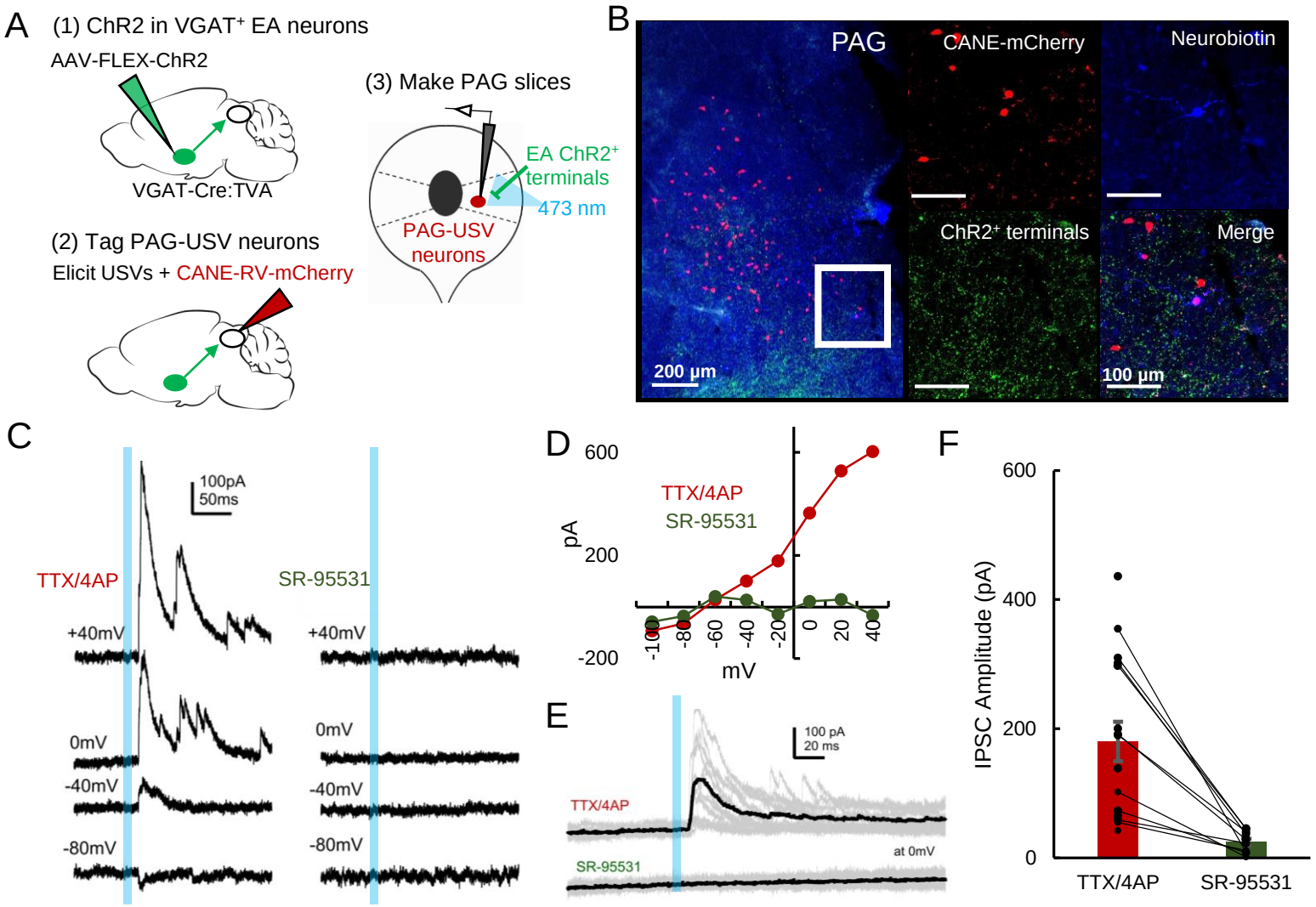

Figure 5: EA_{PAG} neurons provide direct inhibition onto PAG-USV neurons. (A) Viral strategy (left) and schematic (right) for whole-cell patch clamp recordings from fluorescently identified CANE-tagged PAG-USV neurons while optogenetically activating EA_{PAG} axons. (B) Example image of overlap of neurobiotin and mCherry-labeled PAG-USV cells with ChR2-expressing EA_{PAG} axon terminals in the PAG. (C) Example of light-evoked IPSCs at different voltages from one PAG-USV cell recorded in TTX/4AP while stimulating EA_{PAG} axons (left). IPSCs were abolished by bath gabazine application (right). (D) The peak magnitude of light-evoked currents at different membrane voltages for the same cell as (C) shows that the current reverses around the reversal potential of chloride and is abolished by gabazine. Currents were identified as IPSCs in this manner based on their reversal behavior and, for a subset of cells, by disappearance in gabazine. (E,F) Light-evoked IPSCs recorded in TTX/4AP (observed in n = 16 of 29 CANE-tagged cells from 9 mice) were abolished by application of gabazine (n = 10 cells also recorded in gabazine, N=10 cells, $p<0.001$, paired t-test). IPSC amplitude refers to the peak of the light-evoked current at 0 mV holding potential. Error bars represent S.E.M.

Figure 6: POA neurons provide direct inhibition onto VGAT⁺ PAG neurons, which provide direct inhibition onto PAG-USV neurons

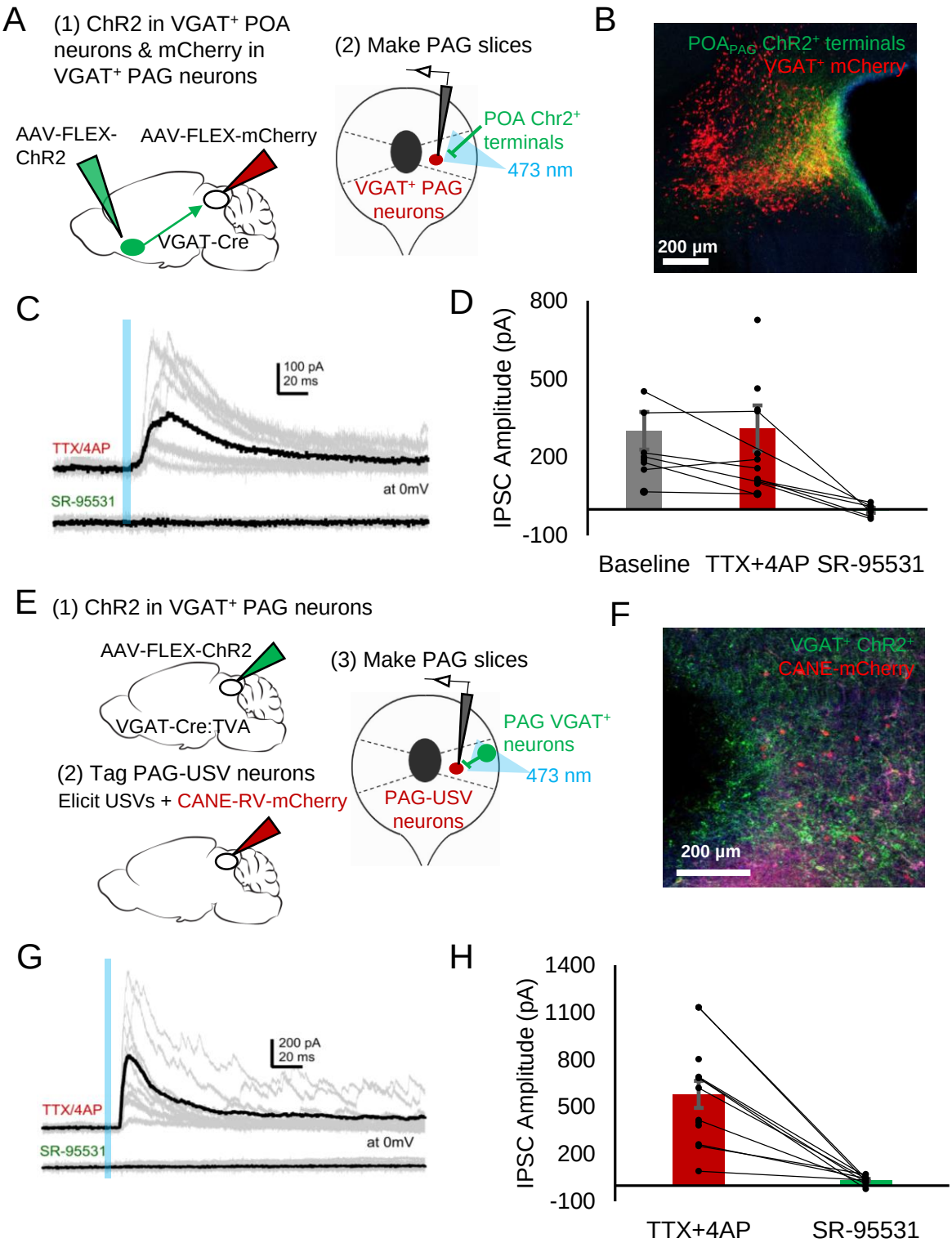

Figure 6: POA neurons provide direct inhibition onto VGAT+ PAG neurons, which provide direct inhibition onto PAG-USV neurons. (A) Viral strategy (left) and schematic (right) for whole-cell patch clamp recordings from fluorescently identified $VGAT^+$ PAG cells while optogenetically activating POA_{PAG} axons. (B) Example image of mCherry-labeled $VGAT^+$ neurons with ChR2-labeled POA_{PAG} axon terminals in the PAG. (C, D) Light-evoked IPSCs (observed in n=18 of 27 $VGAT^+$ neurons recorded from 8 mice) persisted in TTX/4AP and were abolished by bath application of gabazine (n=16 cells recorded in TTX/4AP, n=6 cells also recorded in gabazine, p=0.06, one-way ANOVA comparing baseline vs. TTX+4-AP vs. SR-95531). IPSC amplitude refers to the peak of the light-evoked current at 0 mV holding potential. Error bars represent S.E.M. (E) Viral strategy (left) and schematic (right) for whole-cell recordings from fluorescently identified CANE-tagged PAG-USV neurons while optogenetically activating local $VGAT^+$ PAG neurons. (F) Example image of mCherry-labeled CANE-tagged PAG-USV neurons and ChR2-labeled $VGAT^+$ PAG neurons. (G,H) Light-evoked IPSCs recorded in TTX/4AP (observed in n = 13 of 16 CANE-tagged cells from 4 mice) were abolished by gabazine application (N=10 cells also recorded in gabazine, $p<0.001$, paired t-test). IPSC amplitude refers to the peak of the light-evoked current at 0 mV holding potential. Error bars represent S.E.M.

Figure 7: Model of bidirectional descending control of the PAG vocal gating circuit

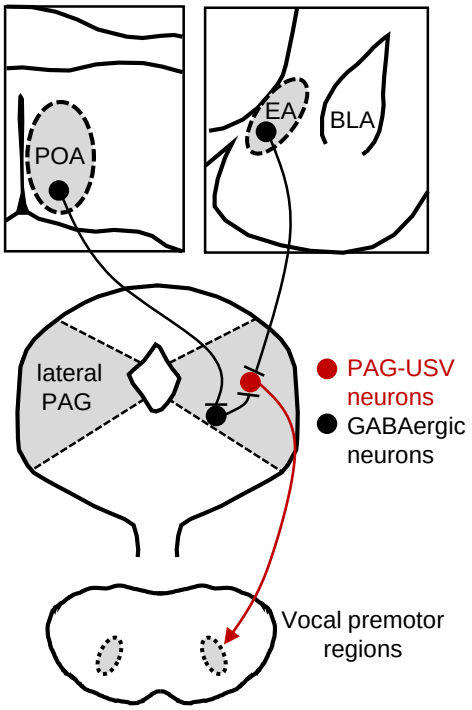

Figure 7: Model of bidirectional descending control of the PAG vocal gating circuit. Inhibitory neurons within the POA provide direct input to inhibitory neurons within the PAG, which in turn provide direct input to PAG-USV neurons. In this manner, activation of POA_{PAG} neurons disinhibits PAG-USV neurons, which provide excitatory input to downstream vocal premotor neurons and drive USV production. Conversely, inhibitory neurons within the EA provide direct inhibitory input to PAG-USV neurons. Hence activation of EA_{PAG} neurons reduces PAG-USV activity and transiently suppresses USV production.